



Discovery of dual cation- π inhibitors of acetylcholinesterase: design, synthesis and biological evaluation

Naresh Damuka¹ · Kurumurthy Kammari¹ · Angamba Meetei Potshangbam^{1,2} · Ravindranath Singh Rathore³ · Anand K. Kondapi¹ · Vaibhav Vindal¹

Received: 18 May 2019 / Revised: 18 February 2020 / Accepted: 25 February 2020
© Maj Institute of Pharmacology Polish Academy of Sciences 2020

Abstract

Background Alzheimer's disease (AD) is a widespread dementia-related disease affecting mankind worldwide. A cholinergic hypothesis is considered the most effective target for treating mild to moderate AD. Present study aims to identify new scaffolds for inhibiting acetylcholinesterase activity.

Methods To find Acetylcholinesterase (AChE) inhibitors, we computationally designed and chemically synthesized a series of cation- π inhibitors based on novel scaffolds that potentially block AChE. The cytotoxic effect of inhibitors were determined by MTT. AChE inhibition experiment was performed by Ellman and the Amplex red method in the SH-SY5Y cell line. Further, the experimental data on designed compounds corroborate with various computational studies that further elucidate the binding mode of interactions and binding affinity.

Results The inhibitors were designed to promote dual binding and were incorporated with groups that may facilitate any of the cation- π , hydrophobic and hydrogen-bonding interactions with the conserved and hot-spot residues in the binding site. The inhibitors possessing pyridine-*N*-methylated pyridinium group and thereby involved in cation- π interactions are highly active relative to the marketed drug Donepezil as well as the designed analogs that lack the group. In vitro enzymatic Ellman assay and Amplex red assay on SH-SY5Y cell line estimated IC₅₀ of the designed compounds in nM range with one having binding affinity higher than Donepezil. Compounds exhibit no significant toxicity up to μ M range.

Conclusions Compounds possessing methylidencyclohexanone scaffolds, with characteristic dual-binding and involving strong cation- π interactions, serves as new leads for AChE and opens a new direction for drug discovery efforts.

Keywords Drug design · 2,6-dimethylenecyclohexanone · AChE · Cation- π interactions

Introduction

Alzheimer's disease (AD) is characterized by a progressively degenerative disorder in the brain, having multifactorial syndromes such as memory loss, progressive impairment in cognitive functions and behavioral impairment.

Several studies have been undertaken to comprehend the molecular pathogenesis of AD. However, the most significant outcome from these studies regarding the pathogenesis of AD, and which are implicated in the drug development. In AD, the main pathological features are grouped into the following categories such as genetic factors [1], aggregation of beta-amyloid in senile plaques [2], neuron-immune dysfunction [2, 3], cerebrovascular dysfunction [4] and cholinergic neurotransmission [5, 6]. Of all these pathogenic events, the cholinergic neurotransmission also known as a cholinergic hypothesis is considered as the utmost effective target for

Electronic supplementary material The online version of this article (<https://doi.org/10.1007/s43440-020-00086-2>) contains supplementary material, which is available to authorized users.

✉ Vaibhav Vindal
vaibhav@uohyd.ac.in

¹ Department of Biotechnology and Bioinformatics, University of Hyderabad, Hyderabad 500046, India

² Department of Biotechnology, Manipur University, Canchipur, Imphal, Manipur 795003, India

³ Department of Bioinformatics, School of Earth, Biological and Environmental Sciences, Central University of South Bihar, Gaya 824236, India

treating AD. The cholinergic hypothesis is based on the observation that AD patients showed a loss of cholinergic activity in their brain. Therefore, it was postulated that the cognitive weakening experienced by AD patients is due to the lack of acetylcholine resulting in inefficient cholinergic neurotransmission. Hence, the inhibition of Acetylcholinesterase (AChE) was considered the most natural therapeutic strategy to reverse the acetylcholine deficiency in AD. Four cholinergic AChE inhibitors such as donepezil, galantamine, rivastigmine, and tacrine are commonly prescribed for the symptomatic treatment of AD.

The active pocket of AChE consists of two regions the 'esteratic' and 'anionic' subsites [7]. The esteratic sites form the catalytic machinery of the enzyme, while the anionic regions are involved in guiding the acetylcholine (ACh) substrate for binding to the conserved residues [8]. At the esteratic subsite, the substrate undergoes hydrolysis by the catalytic triads consisting of Ser203, His447 and Glu334 residues [9]. Additionally, AChE possesses several subsites such as Peripheral Anionic Subsite (PAS) [10, 11] comprising of Asp74, Tyr124, Ser125, Trp286, Tyr337 and Tyr341, oxyanion hole [12] (Gly121, Gly122, Ala204), anionic subsite [13] (Trp86, Tyr133, Glu202, Gly448, Ile451) and acyl binding pocket [14] (Trp236, Phe295, Phe297, Phe338).

PAS provides a transitional binding site of the ACh substrate [15–17]. The residue Trp286 plays a critical role in ligand binding using a combination of steric and electrostatic blockade via the gorge by altering the catalytic rate and catalytic triad conformation [18]. The anionic pocket is located next to the catalytic site, where the conserved residue Trp86 plays a very significant role in guiding the substrate to the active site [14, 19]. The acyl binding pocket binds to the acetyl group of AChE is formed by the residues Phe295, Trp236, Phe297 and Phe338 [14]. The positively charged quaternary ammonium group of the substrate forms cation- π interactions [14]. These interactions lead to substrate recognition and catalytic mechanism of the enzyme [9].

AChE is also involved in several noncatalytic activities [20, 21], for example, the development of AD plaque by promoting A β accumulations [15]. Further, it has been reported that AChE inhibitors capable of interacting with both the catalytic sites and PAS were able to prevent A β accumulation [15, 22]. Therefore, dual binding AChE inhibitors may provide effective treatment of AD, eventually leading to the development of Donepezil and other drugs currently prevalent in the market.

Despite the availability of Rivastigmine (Exelon), Memantine (Namenda), Galantamine (Razadyne), Donepezil (Aricept) and Tacrine, the prolonged treatment, multiple side effects and various studies questioning the sustained efficacy of these drugs necessitated exploration of a new set of potent and effective drugs. Towards this direction, the knowledge of protein–ligand interactions could be exploited

for designing new drugs. The X-ray crystal structures of AChE with diverse inhibitor complexes revealed significant insight into structural features critical for designing new drug molecules.

In this study, we have designed a series of inhibitors based on novel scaffolds that potentially block AChE in dual binding fashion incorporating functional groups that promote cation- π , hydrogen bonding and hydrophobic interactions with the conserved and hot-spot residues.

Materials and methods

The Ala scan was performed on AChE-Donepezil complex (PDB ID: 4EY7) using the Residue Scanning module in Bioluminate (Schrödinger). The method calculates relative binding affinity values (ΔG_{bind}) between the mutant and the wild type using implicit solvation based MM-GBSA approach and stability ($\Delta G_{\text{stability}}$) is calculated using the thermodynamic cycle approach. ΔG_{bind} or Δ Affinity is the change in binding affinity between binding partners upon mutation. A negative value refers that the mutant binds better. The calculations were carried out using the Schrodinger Prime program with an implicit solvent term [23]. $\Delta G_{\text{stability}}$ or Δ Stability (solvated) is the change in the stability of the protein upon mutation, calculated using the Prime energy function with an implicit solvent term. The stability was defined as the difference in free energy between the folded state and the unfolded state. A negative value refers that the mutant is more stable [23].

Chemical synthesis and characterization

All reagents and solvents were obtained from Aldrich and Merck and were spent on chemical synthesis and characterization. The ^{13}C -NMR and ^1H -NMR spectrum were recorded at Bruker 500 MHz and 400 MHz spectrometer, respectively. The chemical shifts are reported in parts per million (ppm). Tetramethylsilane (TMS) and DMSO- d_6 used as an internal standard and solvent, respectively. Platinum-ATR-IR, Bruker spectrometer, Germany managed by Bruker OPUS 7.0 software, was used to record Infrared spectra (IR), in the range of 500–4000 cm^{-1} . Approximately 2 mg of the compound was used for spectra recording and absorbance was generated by signal averaging 64 scans with a resolution of 4 cm^{-1} and the spectra were obtained as wave number versus absorbance units. High-resolution mass spectra (HRMS) were noted on micromass ESI-TOF MS. TLC was done on percolated silica gel plates (Kieselgel 60,254, E.Merck, Germany). Chromatograms were analyzed by UV at 254 nm and 365 nm, followed by iodine vapors. Kofler hot stage device was used to analyse melting points.

General method for the chemical synthesis of compounds

1–3

The chemical synthesis was performed as previously described [24]. Briefly, Pyridine aldehyde (4 mmol) and cyclohexanone (2 mmol) were mixed in 20 ml distilled water. The solution was then stirred in 2 ml of ice-cold Sodium hydroxide (10%) for 10 h. Further, the solution was neutralized with dilute HCl leading to the formation of a precipitate that was filtered carefully. Ethanol was used to recrystallize the precipitate and the pure compound was recovered by column chromatography using ethyl acetate/hexane solution [25].

General method for the chemical synthesis of compounds

1A, 2A and 3A

The compounds were synthesized as per the protocol described elsewhere [26]. Briefly, 2,6-Bis(pyridinylmethylene)cyclohexanone (2 mmol) derivatives were dissolved in acetonitrile (10 ml) and immediately cooled to 5 °C in a 25 ml round bottom flask. 5 ml of Methyl Iodide solution was injected into the flask using a syringe. The entire mixture was stirred first at 5 °C for 12 h, followed by RT for 72 h. The compound precipitate was filtered and washed with little acetonitrile.

In vitro activity and toxicity Assays

Chemicals

F12 medium, Eagle's minimum essential medium (EMEM), pen-strep solution and FBS, were obtained from Gibco-Thermo Fisher Scientific. The Amplex® Red Acetylcholine/Acetylcholinesterase assay kit (A12217) was obtained from Thermo Fisher Scientific. Acetylcholinesterase (AChE), 5,5-Dithiobis-2-nitrobenzoic acid (DTNB) and acetylthiocholine iodide (ATCI). MTT and resorufin sodium salt were procured from Sigma-Aldrich. Dipotassium hydrogen phosphate (K_2HPO_4) and Potassium dihydrogen phosphate (KH_2PO_4) were purchased from Molychem.

Cell culture

SH-SY5Y neuroblastoma cell vial was taken from NCCS (National Center for Cell Science, Pune, India). The SH-SY5Y cells were cultured in a 45% EMEM medium, F12 medium (45%) and 10% FBS, at 37 °C, 5% CO_2 .

Enzymatic Ellman's assay

Compounds **1**, **2**, **3** were dissolved in dimethyl sulfoxide (DMSO) and **1A**, **2A**, **3A** compounds were prepared in

water. Each of the molecules was diluted to various concentrations immediately before use. Donepezil was used as a positive control. Ellman's modified colorimetric method was used to evaluate AChE inhibitory activity [27]. The assay procedure contained sodium phosphate buffer (0.1 M), DTNB (0.3 mM), AChE enzyme from *Electrophorus electricus* (0.01 U) and ATCI (0.5 mM). Various concentrations were evaluated for each chemically synthesized compound in triplicate to get the range of 15% and 90% inhibition for AChE. Each tested compounds were mixed to the assay solution and incubated at 37 °C for 10 min. After that period, ATCI substrate was added. The rate of absorbance change was measured at 405 nm for 5 min on a microplate reader Tecan infinite M 200 pro. The values of IC_{50} were calculated from the absorbance at 405 nm.

MTT assay

To investigate cellular toxicity, 10,000 SH-SY5Y cells were cultured in 96-well plate. After 24 h, different concentrations of test ligands were added and maintained at 37 °C and 5% CO_2 for 24 h. After the test ligands treatment, the remaining media, including test compounds, were discarded. Again 100 μ l of media and 20 μ l of 5 mg/ml MTT solution were added to each well and further maintained for 4 h at 37 °C. The media was carefully discarded and 200 μ l of DMSO was added. MTT formazan product was ascertained by calculating absorbance with an ELISA reader at 570 nm wavelength by Tecan infinite M 200 pro. The untreated cells were defined as 100%.

Amplex red cellular assay

Amplex red Acetylcholinesterase inhibition assay was evaluated by using the Amplex® Red Acetylcholine/Acetylcholinesterase Assay Kit (A12217) method obtained from Thermo Fisher Scientific. Briefly, 6000 viable SH-SY5Y cells were seeded into black 96 well plate and maintained at RT with a 200 μ l reaction mixture possessing 100 μ M ACh, 50 μ M Amplex Red; 0.25 U/mL choline oxidase, 1.0 U/mL horseradish peroxidase. The rate of Fluorescence of resorufin (λ_{ex} = 544 nm; λ_{em} = 590 nm) was calculated at 60 min with a microplate reader Tecan infinite M 200 pro.

In silico study

Molecular docking

Molecular docking investigation was done using Glide program [28] of Schrödinger Suite. Protein structure complex was pre-processed before docking study by Protein Preparation Wizard. Since no conserved water molecules

were observed in the crystal structure water molecules were completely deleted. To maintain the suitable ionization states for the basic and acidic amino acid residues, hydrogen atoms were included at pH 7.0. Further, the maximum possible positions for –SH and –OH hydrogen atoms were selected and proper assignment of the protonation states and tautomers of His as well as Chi ‘flip’ for His, Gln and Asn amino acid residues were also performed. RMSD (Root mean square deviation) value of 0.30 Å was taken to avoid steric collisions among the residues. The OPLS-2005 force field was used for energy minimization.

The inhibitors were made using the Maestro builder panel. 3D structures were made using the Ligprep unit in Schrödinger. The OPLS-2005 force field was used for computing partial atomic charges. The correct bond length and angles, as well as chiralities, tautomers, stereo chemistries, ring conformation and ionization state at pH 7.0, were obtained using Ligprep. To generate energy-minimized 3D structures, the OPLS-2005 force field was used with 0.01 Å RMSD cutoffs.

Molecular docking of the designed inhibitors was performed on the human AChE crystal structure in complex with Donepezil (PDB ID: 4EY7 resolution, 2.35 Å). There was 88% sequence identity and an RMSD of 0.394 Å at the binding site (within a distance of 5 Å from ligand binding site) (supplementary Fig. 1) with the other PDB ID (1C2O, 1C2B and 1EEA from *Electrophorus electricus*) having a resolution of 4.2–4.5 Å.

Grid box was generated around the co-crystallized drug molecule of AChE (PDB ID: 4EY7) active site with a grid box size of 20 × 20 × 20 Å. The van der Waals scaling was kept as default and the partial charges were given from the force field. All the designed inhibitors interacted into the active pocket described by the Grid generation protocol implementing Glide XP (extra precision). Glide scoring function is used to estimate the binding affinity of protein–ligand docking poses. The funnel-type approach was included in the glide algorithm to carry out an efficient search of orientations, conformations, and positions of the ligand in the active site of the protein. Maestro’s pose viewer was used to analyze the output files.

Re-docking, the extracted co-crystallized drug from the binding site serves as one way of validating the reliability of the molecular docking procedure, implemented in the present study. The RMSD between the co-crystallized Donepezil and the binding orientation obtained from its re-docking into AChE active site was found to be less than 1 Å. It results in a similar binding pose as shown in supplementary Fig. 2, validating the reproducibility of the docking procedure.

Molecular dynamic simulation

The molecular dynamics simulations of the Apoenzyme and AChE-inhibitor complexes were done using Desmond [29]. OPLS-AA 2005 force field was used in molecular dynamics simulations [29, 30]. The apoenzyme and complexes were solvated with TIP3P water model as the protein and ligands were already prepared in the docking process. An orthorhombic periodic boundary box was chosen for subsequent MD simulations. To preserve charge neutrality of the system, proper numbers of counter ions were included. The distance between the wall and box was fixed greater than 10 Å to prevent direct binding with its own protein complex. The steepest descent process was implemented to reduce the potential energies of the systems by setting greater than 5000 steps with a 25 kcal/mol/Å gradient threshold. This ensued through L-BFGS minimizer until 1 kcal/mol/Å convergence criteria were attained.

Default parameters provided in Desmond were used for pressure and temperature equilibrations. The MD simulations were carried out for 50 ns at 300 K constant temperature and 1 atm constant pressure with a 2 fs time step of on the equilibrated systems. Particle-mesh Ewald PME method (particle-mesh Ewald) [31] was used to give 0.8 Å grid spacing for long-range electrostatic interactions. Short-range electrostatic and Van der Waals interactions were efficiently shortened at 9.0 Å.

Binding free energy

The Prime MM-GBSA technique, implemented in Schrödinger [23, 32], was used to analyze the free energy of the simulation trajectories of the complexes. The binding energy was estimated for an entire of 100 frames of the MD trajectory. The calculation of the MD trajectory started from the last 25 ns stable simulation until the finish of the trajectory. According to the following equation, the binding free energy was estimated.

$$\Delta G_{\text{Bind}} = \Delta E_{\text{MM}} + \Delta G_{\text{Solv}} + \Delta G_{\text{SA}}$$

- ΔE_{MM} is the energy change between the ligand–protein complexes and sum of the energies of the protein and ligand.
- ΔG_{Solv} is the change in GBSA solvation energies of the ligand–protein complex and the sum of the solvation energies for the protein and unbound ligand.
- ΔG_{SA} is the change in surface area energy for the ligand–protein complex and sum of the surface area energies for protein and ligand.

Statistical evaluation

The IC_{50} inhibitory concentrations were ascertained using GraphPad Prism software v. 7 by studying the log of the dose–response curves by nonlinear regression analysis.

Results

Hot-spot residues in binding site and design of cation- π inhibitors

To design the new series of inhibitors, initially, hot-spot residues were identified using the ALA scanning approach implemented in Schrödinger-Bioluminate [23]. The quantitative assessment of the contribution of each residue to the binding affinity and stability is shown in Table 1. A residue was considered a hot-spot residue if its mutation to alanine yielded loss in binding affinity greater than 2 kcal/mol [33]. The substantial losses of affinity upon ALA mutations were observed for residues Trp286, Tyr341, Phe338 and Trp86 (supplementary Fig. 3). These hot-spot residues were targeted primarily for designing the new inhibitors. Further, the X-ray structure of AChE-ACh complexes (PDB ID: 2HA5 and 2HA4) revealed that the quaternary ammonium of acetylcholine not only has cation- π interaction with Trp86 at the anionic site but also with Trp286 at the PAS as shown in supplementary Fig. 4. This signifies the critical role of Trp86 and Trp286 in enzyme catalytic activity through cation- π interactions. Another important criterion that we considered for designing the new cation- π inhibitors was inspired by the characteristic dual binding drug such as Donepezil, which mainly interacts with the enzyme through hydrophobic groups. Accordingly, the two ends of the inhibitors were prepared using pyridine-*N*-methylated pyridinium moiety, thereby introducing positive group as well as the hydrophobic moiety. The linker group prominently as hydrophobic was constructed with 2,6-dimethylenecyclohexanone moieties. This group is intended to bind with the Acyl binding pocket of the enzyme.

Overall, inhibitors have pyridine-*N*-methylated pyridinium moiety similar to acetylcholine quaternary ammonium moiety. It also possesses aromatic groups at both ends and a linker group in the middle. To understand the critical role of positive ions in the molecule, a series of inhibitors similar to the cation- π inhibitors were also designed, without the positive group.

Synthetic chemistry

The pyridine-*N*-methylated of 2,6-bis(pyridinylmethylene)cyclohexanone derivatives were prepared by implementing the synthetic route, as shown in Schemes 1 and 2. The

inhibitors without positive ions were prepared following the procedure in Scheme 1 routine. Compounds 1–3 were prepared by aldol condensation of various pyridine aldehydes with cyclohexanone in the presence of 10% aqueous sodium hydroxide. Compound 1A–3A was prepared by pyridine *N*-methylation of Scheme 1 products in the presence of methyl iodide, as depicted in Scheme 2.

The new type of proposed inhibitors are shown in Table 3. The biological activities of each of the molecules were evaluated by Ellman's and amplex red biological assay. Further, molecular docking and molecular dynamics studies were held to understand the molecular mechanism of the binding interaction of the inhibitors at the AChE active site.

Molecular activity

To determine the inhibitory effect of the designed and synthesized novel type ligands, *In vitro* AChE inhibition assays were performed according to Ellmann's method. Donepezil was utilized as a reference compound for the inhibitory evaluation. The initial screening of the AChE inhibitory effects of the synthesized compounds was performed at 100 μ M concentration. Compounds 1, 2, 3 have failed to exhibit AChE inhibitory activity, as shown in Fig. 1.

The lack of inhibitory activity of chemically synthesized compounds 1, 2 and 3 is attributed to the lack of positive charge group in pyridinyl moieties, which is necessary for cation- π interactions at the enzyme active site. However, when the positive group is introduced in compound 1A, 2A and 3A, the inhibitory activity was observed in the nanomolar range. The quaternary ammonium at the Para position of compound 1A has $IC_{50} = 20.9$ nM, arguably due to cation- π

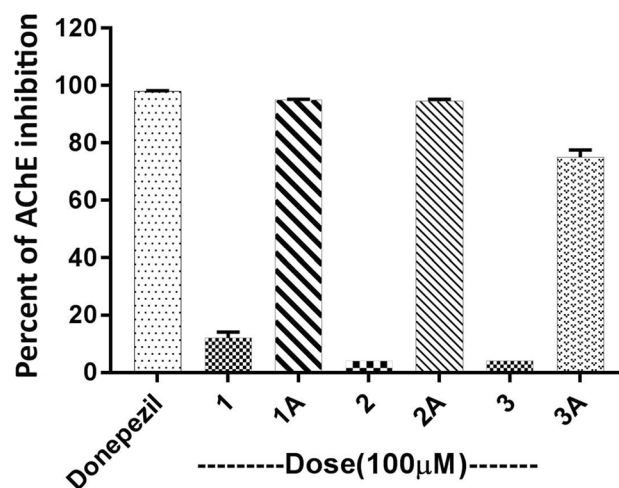


Fig. 1 The effect of compounds 1–3 and 1A–3A on AChE inhibitory activity. All experiments on three different test materials were conducted at the same time using Donepezil as a single positive control. Error bars represent mean \pm SD; $n = 3$

interactions with the conserved residues Trp86 and Trp286 at the enzyme active site. Compound **2A** with the Meta positioned quaternary ammonium has the highest activity ($IC_{50}=6.2$ nM), again due to proximity and thereby strong interaction with the conserved residues (Trp86 and Trp286). The quaternary ammonium at ortho position (in compound **3A**), wherein the cation group faces the opposite side of π moiety in Trp86 and Trp286 fails to participate in cation- π interaction leading to lesser activity.

In addition to Ellmann's method, which was carried out in the presence of a pure enzyme, the potency of the **1A**, **2A**, and **3A** were also assessed by Amplex red assay in neuronal SH-SY5Y cell lines. In the amplex red assay, AChE activity is monitored by highly fluorescent product resorufin, which is easily measured in fluorescence emission spectroscopy. According to Amplex red AChE inhibitory assay, **1A** and **2A** compounds showed high activity for AChE inhibition in the nanomolar range and **3A** compound demonstrated a less inhibitory activity that corroborates with Ellman's data. Compound **2A** was discovered to have the most potent inhibitory activity with IC_{50} values of 4.4 nM and noticeable observation is that its activity is even higher than that of Donepezil. ($IC_{50}=9.0$ nM). The IC_{50} values of **1A**, **2A**, and **3A** are represented in Table 2.

Molecular toxicity

The cytotoxic effect of the newly designed and synthesized compounds was determined in SH-SY5Y, a human neuroblastoma cell line. In the MTT assays, the treatment of SH-SY5Y with **1A**, **2A** and **3A** at increasing concentrations (0.6 μ M to 8 μ M) for 24 h did not show significant

Table 1 Relative binding affinity and stability between wild type and mutated residues

Sl. No	Residue ^a	Mutated ^b	Δ Affinity ^c	Δ Stability (solvated) ^d
1	Trp286	ALA	11.55	11.60
2	Tyr341	ALA	10.18	11.67
3	Phe338	ALA	5.39	12.10
4	Trp86	ALA	3.96	12.63
5	Tyr72	ALA	3.12	9.39
6	Phe297	ALA	2.87	14.01
7	Tyr337	ALA	2.10	6.23
8	Tyr124	ALA	2.01	9.54
9	Ser203	ALA	1.33	10.72
10	His447	ALA	1.05	0.21
11	Val294	ALA	0.74	12.27
12	Ile451	ALA	0.21	18.53
13	Arg296	ALA	0.17	29.15
14	Leu289	ALA	0.02	13.06
15	Ser293	ALA	-0.06	0.91
16	Tyr133	ALA	-0.43	21.78
17	Phe295	ALA	-1.89	11.22
18	Asp74	ALA	-2.44	-3.41
19	Glu202	ALA	-5.25	-8.99

^aOriginal residues

^bMutated residues

^cCalculated binding affinity

^dCalculated stability

cytotoxicity. Compounds **1**, **2**, and **3** have demonstrated considerable cytotoxicity compared to their pyridine-*N*-methylated pyridinium analogs **1A-3A** (Fig. 2a, b).

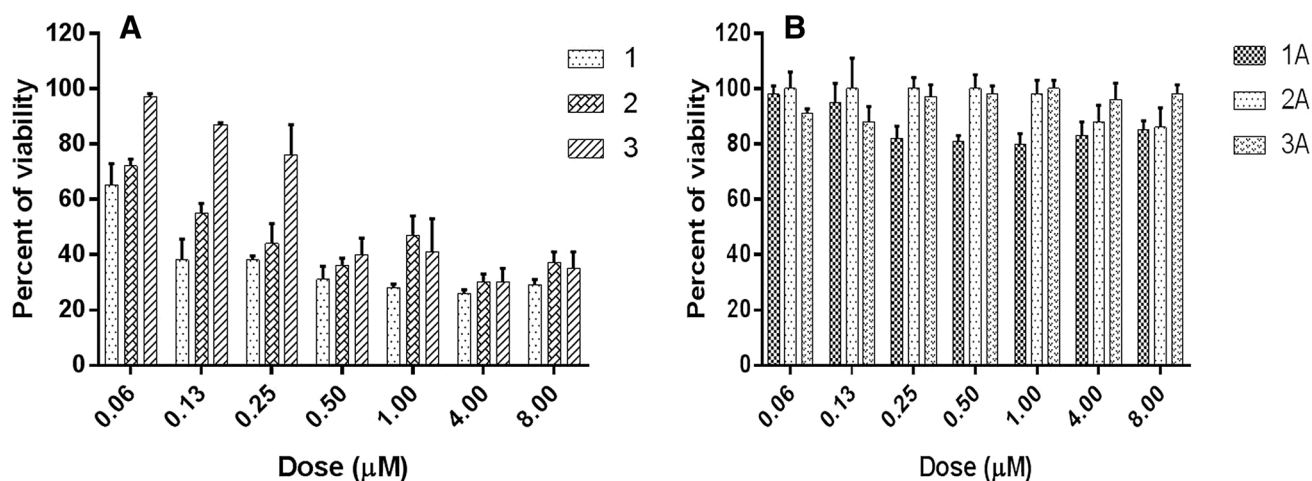
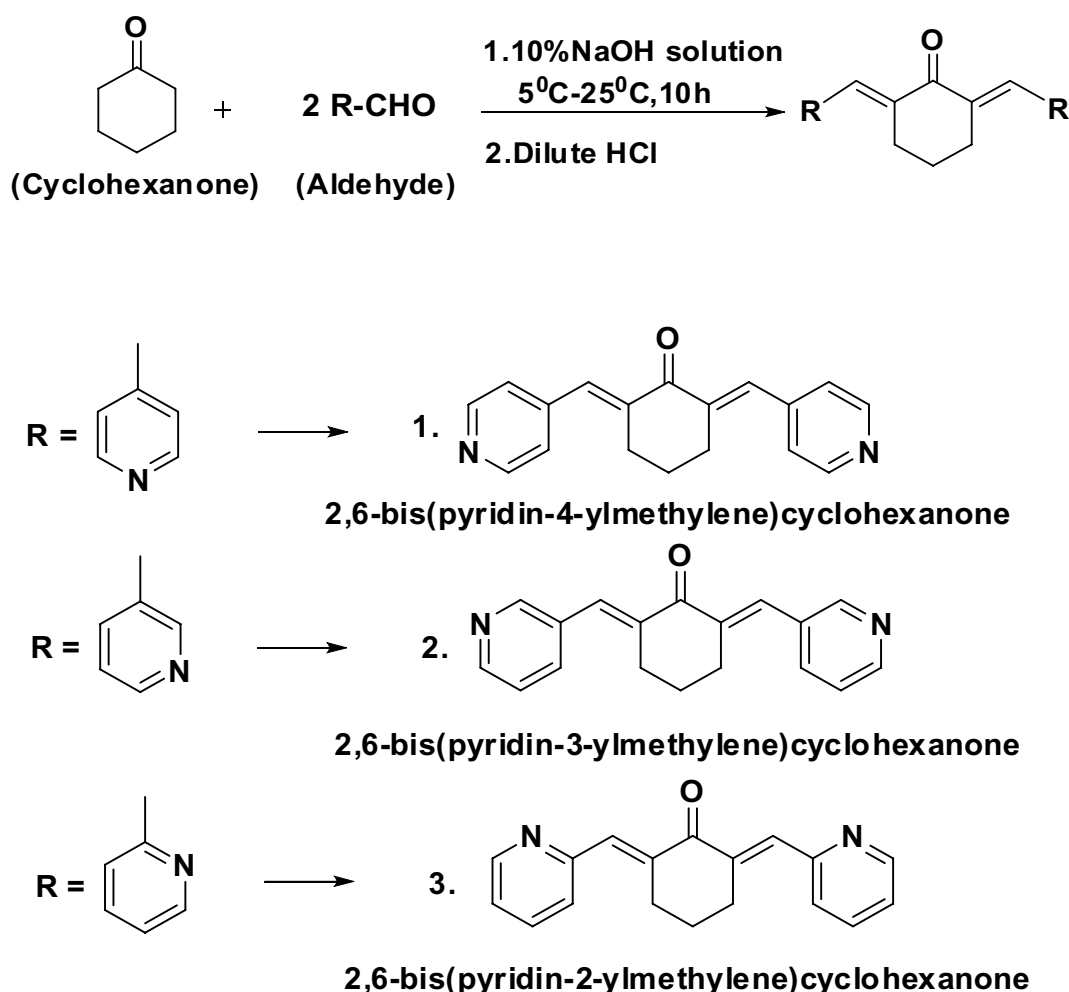


Fig. 2 a, b Effect on Cell viability of SH-SY5Y Cells at different concentrations (0.06 μ M–8 μ M) of compounds 1–3 (a) and **1A-3A** (b) for 24 h. Cell viability was determined with MTT assay. The

experiment was performed in triplicates. The data represent the percentage of viability cells (means \pm SD)



Scheme 1 Preparation of 2, 6-bis(pyridinylmethylene)cyclohexanone derivatives

Binding mode and interactions

Docking analysis

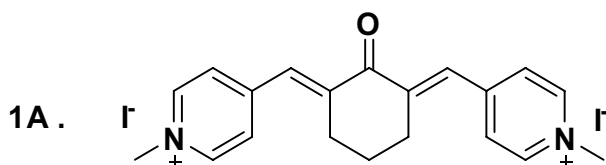
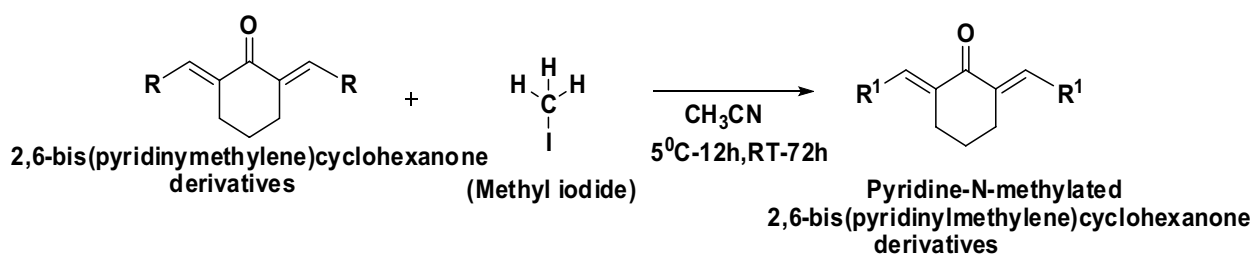
Molecular docking studies of the designed molecules were carried out to delineate a key set of interactions that govern the activity of AChE. The XP docking score and binding residues of the inhibitors are given in Table 3.

Molecule **1A** has a high XP docking score of -13.398 kcal/mol and the binding orientation to the critical residues of AChE active site is presented in Fig. 3. The Para positioned pyridine-*N*-methylated pyridinium group is firmly bound to the anionic sub site, acyl binding pocket and PAS by stacking against Trp86 (Pyrrole: 4.83 Å, Benzene: 5.91 Å), Phe338 (6.65 Å) and Tyr337 (4.81 Å) forming cation- π interactions with the aromatic residues, respectively. Hydrogen bond interaction was also observed at the acyl binding site between the carbonyl group of the linker

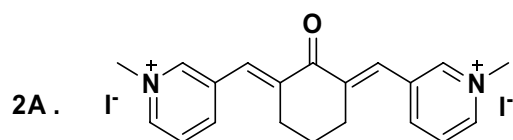
moiety of compound **1A** and the backbone atom of Phe295 (O...HN distance: 1.93 Å).

Similarly, for designed molecule **2A** (with the highest XP docking score of -13.727 kcal/mol), at the anionic sub site, acyl binding pocket and PAS the meta-positioned quaternary ammonium is stacked with the aromatic residues Trp86 (Pyrrole: 5.55 Å, Benzene: 6.38 Å), Phe338 (5.46 Å) and Tyr337 (4.19 Å) making cation- π interactions with the positively charged nitrogen and the aromatic groups, respectively (Fig. 4). Further, at the acyl binding site, similar hydrogen bond interaction was found between the carbonyl oxygen of the linker moiety and the backbone of Phe295 (O...HN, distance: 2.00 Å).

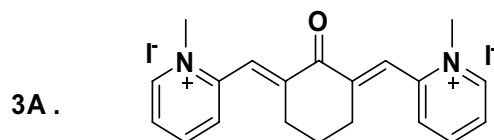
The pyridine-*N*-methylated pyridinium group of **2A** further interacts at the PAS by stacking against the residue Trp286. It allows the positive charge meta-substituted nitrogen of quaternary ammonium to form cation- π interaction as well as π - π interaction, which further stabilizes the complex.



4,4'-(1*E*,1'*E*)-(2-oxocyclohexane-1,3-diylidene)bis(methan-1-yl-1-ylidene)bis(1-methylpyridinium) iodide



3,3'-(1*E*,1'*E*)-(2-oxocyclohexane-1,3-diylidene)bis(methan-1-yl-1-ylidene)bis(1-methylpyridinium) iodide



2,2'-(1*E*,1'*E*)-(2-oxocyclohexane-1,3-diylidene)bis(methan-1-yl-1-ylidene)bis(1-methylpyridinium) iodide

Scheme 2 Pyridine-*N*-methylation of 2,6-Bis(pyridinylmethylene)cyclohexanone

The higher inhibitory activity of **2A** as compared to **1A**, observed in both types of in vitro assays, can be explained according to the predicted interactions at the active site. The meta-positioned quaternary methylated pyridinium allows the binding of the molecule with the key aromatic residues (Trp86, Phe295 and Trp286) at the anionic sub site, acyl binding pocket and PAS. However, Para positioned directs the quaternary methylated pyridinium away from the aromatic residue Trp286 at the PAS, resulting in less interaction and thus less experimental inhibitory activity.

In the case of molecule **3A**, at the anionic subsite, the ortho-positioned quaternary methylated pyridinium is

directed away from the crucial residue Trp86 (Fig. 5), which may provide the reason for lower inhibitory activity as observed in the inhibitory assay. However, cation- π as well as π - π interactions with residues Tyr337 (cation- π distance: 4.49 Å and π - π distance: 5.12 Å) and Phe338 (cation- π , distance: 4.28 Å) were observed at PAS and acyl binding pocket, respectively. Further, at the acyl binding pocket site, the same hydrogen bond interaction is formed between the carbonyl oxygen and Phe295 (O...HN, distance: 1.95 Å). At the PAS, another π - π interaction was observed with pyridine-*N*-methylated pyridinium group by stacking against Trp286 with a distance of 4.3 Å

Table 2 Acetylcholinesterase inhibitory activities of **1A**, **2A** and **3A** compound

Compounds	AChE inhibition IC50 (nM) ^a (Ellman's method)	AChE inhibition IC50 (nM) ^b (Amplex red assay)
1A	20.9 ± 4.2	67.9 ± 2.2
2A	6.2 ± 2.06	4.4 ± 0.8
3A	N/A	N/A
Donepezil	8.5 ± 0.8	9.0 ± 2.3

^aThe inhibition activities of AChE were screened by Ellman's method. IC50 values are means ± standard deviation of three independent experiments

^bAmplex red Assay performed using SH-SY5Y cells. IC50 values are means ± standard deviation of duplicate independent experiments

from the rings. Molecule **3A** also has a lower docking score (− 10.29 kcal/mol) as compared to **1A** and **2A**.

The docked conformations obtained from molecular docking for molecules **1**, **2**, and **3**, are shown in Fig. 6. Molecule **1**, **2**, and **3** failed to demonstrate the dual binding mode. However, they are able to participate in hydrogen bonding interactions at the acyl binding pocket with Phe295. The absence of cation- π interactions for these compounds might have resulted in the loss of activity in the experimental assays.

Table 3 Docking result of the synthesized molecules with AChE

No	Compound	XP GScore ^a (kcal mol ⁻¹) ^a	Binding residues ^b
1		-9.272	PHE295
2		-9.442	PHE295
3		-9.536	PHE295
1A		-13.398	PHE295, TRP86, TYR337, PHE338
2A		-13.727	PHE295, TRP286, TRP86, PHE338
3A		-10.219	PHE295, TRP286
Donepezil		-11.234	PHE295, TRP286, TRP86, PHE338

^aGlide XP Docking score of the compounds

^bAChE residues which were predicted to be interacting with the compounds

Dynamics of the enzyme-inhibitor complex: RMSD curves

The molecular dynamics study was carried out to study the behavior of the predicted complexes, considering the inherent flexibility involved in the enzyme. Further, the stability of the molecular interactions predicted by the docking method was examined by monitoring the percentage occurrence of the interactions during the simulation period.

The stability of the simulation system was explored by analyzing the RMSDs of the proteins from the starting structure. As shown in Fig. 7, after initial fluctuation, the C ^{α} -RMSD value of Apo-enzyme (in Donepezil, and designed Para, Meta and Ortho positioned quaternary pyridinium inhibitor complexes) reached a relatively stable conformation after 25 ns, with an average RMSD value of 2–2.4 Å. Similarly, for the ligands bound to the protein, namely Donepezil, **1A-3A**, the RMSDs are shown in Fig. 8. Para and Meta positioned quaternary pyridinium compounds (**1A** and **2A** respectively) showed small fluctuations initially but stabilized at around 2.5 Å throughout the simulation. The study indicates the preserved binding mode of interactions arising out of stable and strong interaction throughout. In the case of Donepezil, the RMSD value was stabilized at around 3 Å at the initial 30 ns, but it further increased to 4.5 Å. The most fluctuation was seen in Ortho positioned quaternary pyridinium compound (**3A**), where three major spikes can be

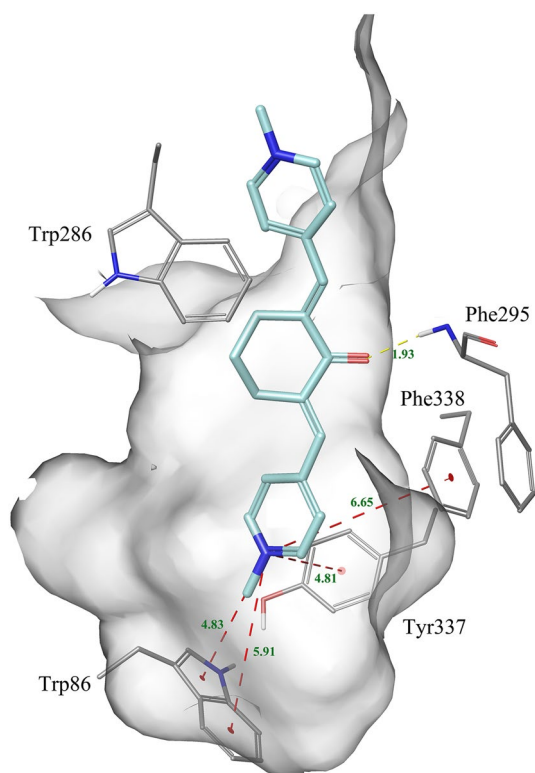


Fig. 3 Binding interaction of compound **1A** at AChE active site shown in turquoise color. Red and yellow dotted lines represent cation- π interactions and hydrogen bonds, respectively. Distance in Å is shown in green

seen reaching around RMSD of 6–7 Å; however, it remained approximately about 5 Å throughout the simulation. The increased flexibility of Donepezil and **3A** could be attributed to fewer interactions with AChE and thereby be highlighting weak binding as compared to **1A** and **2A**, as also observed in both enzymatic and cell line assays.

Binding interactions analysis

In the docking study, the Para substituted methylpyridinium group of molecule **1A** was stacked against Trp86, Tyr337, and Phe338, forming cation- π interactions with the aromatic residues. The Trp86 was preserved in 80% of the simulation time (supplementary Fig. 5). A new hydrophobic π - π interaction was also observed for 47% of the simulation period with Tyr341. In the case of **2A**, the Meta positioned quaternary ammonium showed cation- π interactions with Trp86, which was also preserved for 79% along the simulation (supplementary Fig. 6). Further, due to the Meta substituted position, the distance between Trp86 and methylpyridinium group of **2A** was closer at 4 Å (Fig. 9), which seems to stabilize the complex considerably as compared to **1A**, thus resulting in more biological activity.

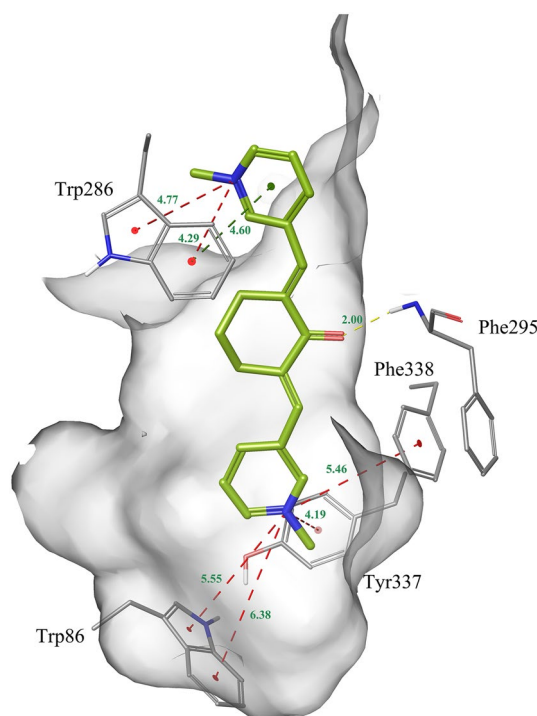


Fig. 4 Binding interaction of compound **2A** at AChE active site shown in yellow-green color. Red, green and yellow dotted lines represent cation- π interactions, π - π interactions and hydrogen bonds, respectively. Distance in Å is shown in green

The least active molecule **3A** having Ortho substituted quaternary ammonium had π - π interaction with Trp86 preserved over 51% of the simulation time, comparatively less percentage of the time with respect to **1A** and **2A** (supplementary Fig. 7).

Free energy analysis using MM-GBSA

The predicted binding free energy obtained from docking and 100 molecular dynamics snapshots complexes calculated using an implicit solvation based MM/GBSA approach are given in Table 4. The plot of approximate binding free energies (ΔG_{bind}) versus the 100 complexes is shown in supplementary Fig. 8. As expected, the most favored binding was exerted by the molecules **1A** and **2A**, having averaged binding free energies (ΔG_{bind}) of $-96.84008 \text{ kcal mol}^{-1}$ and $-94.9527 \text{ kcal mol}^{-1}$ respectively. The Donepezil-AChE complex has slightly lower average binding energies ($-89.25343 \text{ kcal mol}^{-1}$) than **1A** and **2A**. The Ortho positioned pyridine-*N*-methylated pyridinium molecule **3A** has the least average binding free energy (ΔG_{bind}) $-63.75939 \text{ kcal mol}^{-1}$, perhaps due to the loss of cation- π interactions. Predicted binding free energy (ΔG_{bind}) is shown in Table 4.

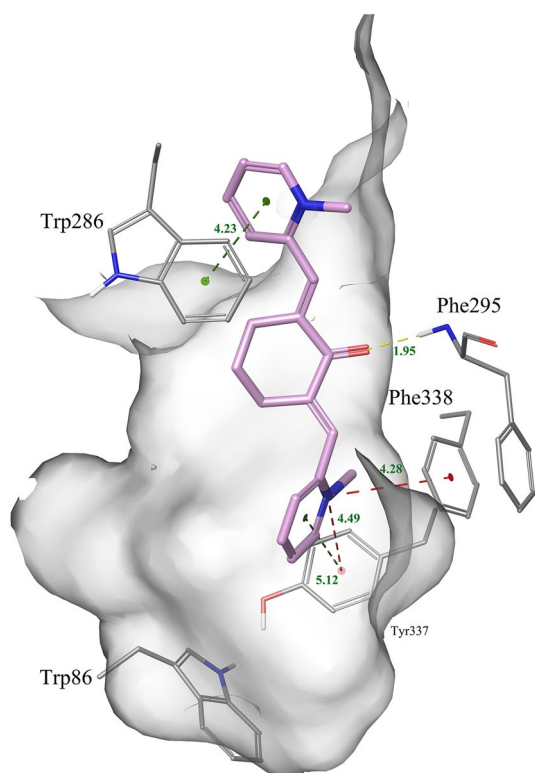


Fig. 5 Binding interaction of compound **3A** at AChE active site shown in plum color. Red, green and yellow dotted lines represent cation- π interactions, π - π interactions and hydrogen bonds, respectively. The distance in Å is shown in green

Active AChE inhibitors **1A**, **2A** and **3A** spectral characterization

Compound **1A**

4,4'-(1E,1'E)-(2-oxocyclohexane-1,3-diylidene)bis(methan-1-yl-1-ylidene)bis(1-methylpyridinium)iodide (**1A**): Yield: 610 mg (99%); m.p.: 196–198 °C; ATR-FTIR (ν cm⁻¹): 3455.97, 3334.04, 3014.65, 1672.74, 1637.77; ¹H-NMR (400 MHz, DMSO-d₆, δ ppm): 9.03 (4H), 8.26 (4H), 7.71 (2H), 4.37 (6H), 3.01 (4H), 1.80 (2H); ¹³C-NMR (100 MHz, DMSO-d₆, δ ppm): 188.72, 151.01, 145.65, 144.26, 131.09, 128.23, 48.14, 28.02, 21.63; HRMS (ESI+): m/z: calculated for C₂₀H₂₂N₂O²⁺(M²⁺): 153.0850; found: 153.0861.

The spectral figures are given in supplementary section (Figs.S9–S12).

Compound **2A**

3,3'-(1E,1'E)-(2-oxocyclohexane-1,3-diylidene)bis(methan-1-yl-1-ylidene)bis(1-methylpyridinium)iodide (**2A**): Yield: 602 mg (98%); m.p.: 230–232 °C; ATR-FTIR (ν cm⁻¹): 3451.9, 3410.8, 3026.5, 2956.4, 2919.7, 2866.7, 1675.0, 1628.8; ¹H-NMR (400 MHz, DMSO-d₆, δ ppm): 9.54

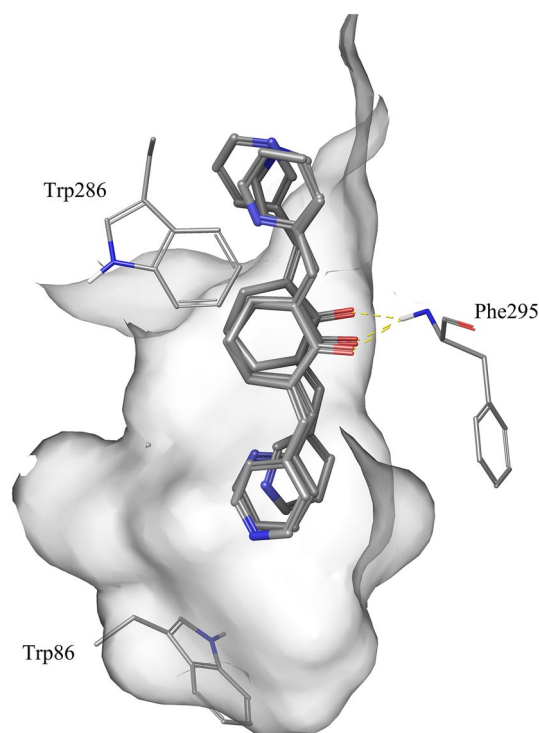


Fig. 6 Binding interaction of compound **1–3** at AChE active site represented as a thick stick in grey color. Yellow dotted lines represent hydrogen bonds

(2H), 9.00 (2H), 8.734 (2H), 8.230 (2H), 7.68 (2H); 4.41 (6H); 3.01 (4H); 1.78 (2H); ¹³C-NMR (100 MHz, DMSO-d₆, δ ppm): 188.44, 146.63, 145.50, 144.98, 141.48, 135.06, 129.64, 127.92, 48.80, 27.86, 22.00; HRMS (ESI+): m/z: calculated for C₂₀H₂₂N₂O²⁺(M²⁺): 153.0850; found: 153.0877.

The spectral figures are given in supplementary section (Figs. S13–S16).

Compound **3A**

2,2'-(1E,1'E)-(2-oxocyclohexane-1,3-diylidene)bis(methan-1-yl-1-ylidene)bis(1-methylpyridinium)iodide (**3A**): Yield: 479 mg (78%), m.p.: 187–189 °C; ATR-FTIR (ν cm⁻¹): 3600.41, 3434.18, 3019.39, 2997.49, 1682.61, 1621.76; ¹H-NMR (400 MHz, DMSO-d₆, δ ppm): 9.19 (2H), 8.64 (2H), 8.15 (4H), 7.66 (2H), 4.29 (6H); 2.85 (4H); 1.77 (2H); ¹³C-NMR (100 MHz, DMSO-d₆, δ ppm): 187.78, 150.65, 147.55, 145.57, 144.90, 129.55, 127.51, 126.43, 46.75, 28.06, 21.82; HRMS (ESI+): m/z: calculated for C₂₀H₂₂N₂O²⁺(M²⁺): 153.0850; found: 153.0892.

Note: Signal multiplicity could not be shown in spectral data. We assumed that due to the di-positivity of molecules, splitting of ¹H-NMR signals was not observed in the spectrum.

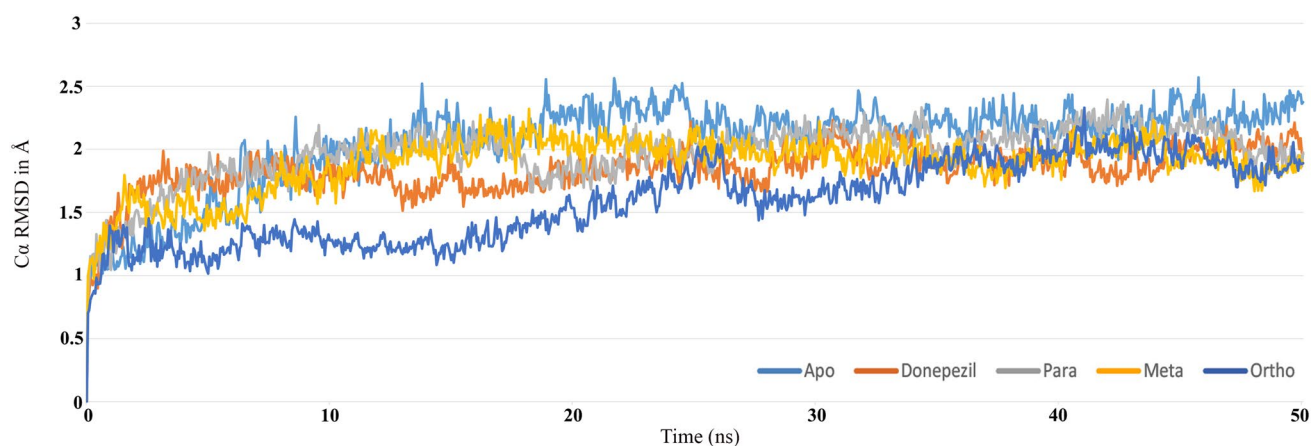


Fig. 7 Root mean square deviation (RMSD) of AChE in the absence (Blue) and presence of bound compounds; Donepezil (Orange), 1A (Grey), 2A (Yellow), and 3A (Dark blue) during the simulation period

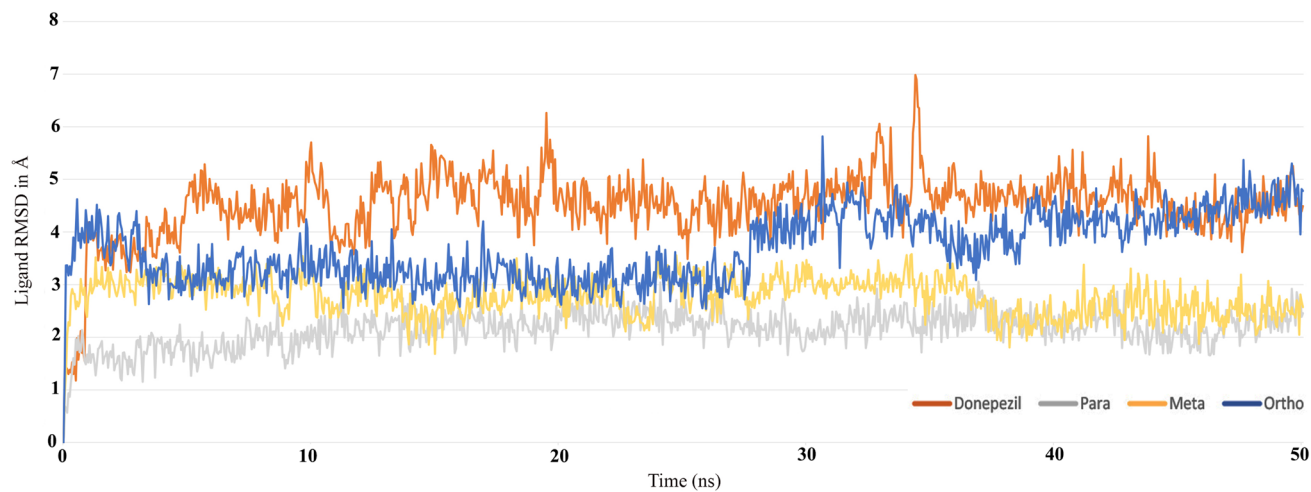


Fig. 8 Ligand Root means square deviation (RMSD) of Donepezil (Orange), 1A (Grey), 2A (Yellow), and 3A (Dark blue) with respect to AChE during the simulation period

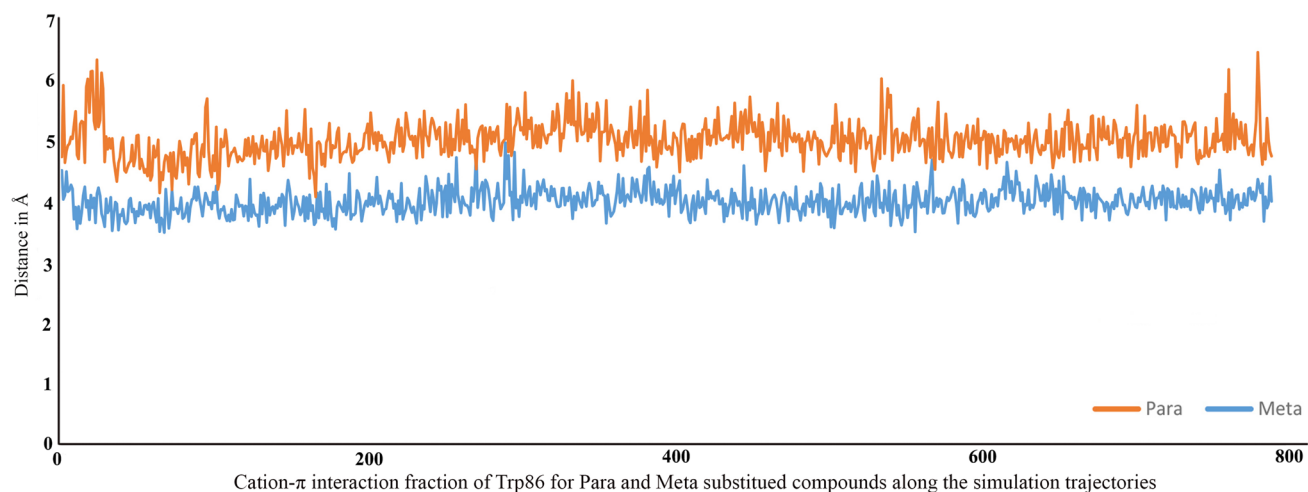


Fig. 9 Plot of cation- π interaction distance (in Å) of compound 1A (Orange) and 2A (Blue) with residue Trp86 during the simulation time

Table 4 Predicted binding free energy (ΔG_{bind}) using MM/GBSA method

Compounds	ΔG_{bind} (Docking) ^a	ΔG_{bind} (MD) ^b
1A	-101.568 kcal mol ⁻¹	-96.84008 kcal mol ⁻¹
2A	-89.074 kcal mol ⁻¹	-94.9527 kcal mol ⁻¹
3A	-57.701 kcal mol ⁻¹	-63.75939 kcal mol ⁻¹
Donepezil	-89.299 kcal mol ⁻¹	-89.25343 kcal mol ⁻¹

^a ΔG_{bind} obtained from docking single inhibitor-enzyme complex^baverage ΔG_{bind} obtained from 100 molecular dynamics snapshots

The spectral figures are given in the supplementary section (Fig. S17–S20).

Discussion

To discover novel and effective drugs for treating Alzheimer's disorder, a series of methylidenecyclohexanone compounds were designed, synthesized. By exploring the active site environment, hot-spot residues of AChE, and exploiting the characteristic dual binding observed in Donepezil, the inhibitors were designed to promote strong cation- π interactions with the conserved residues (Trp86 and Trp286) as well as hydrophobic and hydrogen bonding interactions with important residues. Accordingly, positively charged pyridine-*N*-methylated pyridinium group was introduced at both the ends of the three inhibitors **1A**, **2A** and **3A**. AChE inhibitory activity of these designed compounds was performed with the pure enzyme (Ellman's assay) and with SH-SY5Y neuroblastoma cell line (Amplex red assay). The designed inhibitors involving pyridine-*N*-methylated pyridinium group to facilitate cation- π interactions demonstrated AChE activity in nM ranges, while compound **1**, **2** and **3** lacking such group were found to be inactive at 100 μM or lower concentration.

Compound **2A** with the Meta substituted quaternary ammonium has the highest activity ($\text{IC}_{50} = 6.2 \text{ nM}$), while the Para substituted compound having compound **1A** has $\text{IC}_{50} = 20.9 \text{ nM}$ and the least active compound is **3A**. Further, docking, molecular dynamics studies helped elucidate binding mode and the key set of molecular interactions responsible for AChE activity. Compounds **1A–3A**, possessing positive charged, may not cross the Blood–brain barrier (BBB). However, there are reports for the successful implementation of biocompatible nanoparticles that can overcome the BBB issues of the ligands. One of the latest reports demonstrated that Fe₃O₄@C nanoparticle linked with small molecules were effectively delivered into a specific subcellular component of the brain and restore the memory in mice [34, 35].

The Compounds 1A-3A, possessing novel 2,6-dimethylene-cyclohexanone scaffolds are entirely different from the

existing drugs available in the market such as Rivastigmine (Exelon®), Memantine (Namenda®), Galantamine (Razadyne®), Donepezil (Aricept®) and Tacrine. These derivatives promote characteristic dual-binding as well as strong cation- π interactions, hydrophobic and hydrogen bonding interactions with hot-spot residues. Thus, these compounds can serve as novel leads for AChE.

Acknowledgements This work was supported in part by UPE Phase-II. Financial support from the DBT fellowship is gratefully acknowledged by DN. Financial support from the DBT-RA Program in Biotechnology and Life Sciences is gratefully acknowledged by PAM. Authors also thank funding support from DST-PURSE, UGC-SAP to Department of Biotechnology and Bioinformatics, University of Hyderabad.

Compliance with ethical standards

Conflict of interest There are no conflicts of interest declared by the authors.

References

- Richens JL, Bramble JP, Spencer HL, Cantlay F, Butler M, O'Shea P. Towards defining the mechanisms of alzheimer's disease based on a contextual analysis of molecular pathways. *AIMS Genet.* 2016;3:25–48.
- Yoon S-S, Jo SA. Mechanisms of amyloid- β peptide clearance: potential therapeutic targets for Alzheimer's disease. *Biomol Ther.* 2012;20:245–55.
- Lombardi V, Garcia M, Rey L, Cacabelos R. Characterization of cytokine production, screening of lymphocyte subset patterns and in vitro apoptosis in healthy and Alzheimer's disease (AD) individuals. *J Neuroimmunol.* 1999;97:163–71.
- Marlatt MW, Lucassen PJ, Perry G, Smith MA, Zhu X. Alzheimer's disease: cerebrovascular dysfunction, oxidative stress, and advanced clinical therapies. *J Alzheimers Dis.* 2008;15:199–210.
- Whitehouse PJ, Price DL, Struble RG, Clark AW, Coyle JT, Delon MR. Alzheimer's disease and senile dementia: loss of neurons in the basal forebrain. *Science.* 1982;215:1237–9.
- Francis PT, Palmer AM, Snape M, Wilcock GK. The cholinergic hypothesis of Alzheimer's disease: a review of progress. *J Neurol Neurosurg Psychiatry.* 1999;66:137–47.
- Nachmansohn D, Wilson IB. The enzymic hydrolysis and synthesis of acetylcholine. *Adv Enzymol Relat Subj Biochem.* 1951;12:259–339.
- Quinn DM. Acetylcholinesterase: enzyme structure, reaction dynamics, and virtual transition states. *Chem Rev.* 1987;87:955–79.
- Sussman JL, Harel M, Frolow F, Oefner C, Goldman A, Tokor L, et al. Atomic structure of acetylcholinesterase from *Torpedo californica*: a prototypic acetylcholine-binding protein. *Science.* 1991;253:872–9.
- Taylor P, Lappi S. Interaction of fluorescence probes with acetylcholinesterase. The site and specificity of propidium binding. *Biochemistry.* 1975;14:1989–97.
- Amitai G, Taylor P. Characterization of peripheral anionic site peptides of AChE by photoaffinity labeling with monoazidopropidium (MAP). In: Massouli J, Bacou F, Barnard EA, Chatonnet A, Doctor BP, Quinn DM, editors. *Cholinesterases: structure, function, mechanism, genetics and cell biology.* American Chemical Society; Washington, DC; 1991: p. 285.

12. Harel M, Quinn DM, Nair HK, Silman I, Sussman JL. The X-ray structure of a transition state analog complex reveals the molecular origins of the catalytic power and substrate specificity of acetylcholinesterase. *J Am Chem Soc.* 1996;118:2340–6.
13. Weise C, Kreienkamp HJ, Raba R, Pedak A, Aaviksaar A, Hucho F. Anionic subsites of the acetylcholinesterase from Torpedo californica: affinity labelling with the cationic reagent N, N-dimethyl-2-phenyl-aziridinium. *EMBO J.* 1990;9:3885–8.
14. Ordentlich A, Barak D, Kronman C, Flashner Y, Leitner M, Segall Y, et al. Dissection of the human acetylcholinesterase active center determinants of substrate specificity. Identification of residues constituting the anionic site, the hydrophobic site, and the acyl pocket. *J Biol Chem.* 1993;268:17083–95.
15. Alvarez A, Opazo C, Alarcón R, Garrido J, Inestrosa NC. Acetylcholinesterase promotes the aggregation of amyloid- β -peptide fragments by forming a complex with the growing fibrils. *J Mol Biol.* 1997;272:348–61.
16. Radić Z, Quinn DM, Vellom DC, Camp S, Taylor P. Allosteric control of acetylcholinesterase catalysis by fasciculin. *J Biol Chem.* 1995;270:20391–9.
17. Barak D, Kronman C, Ordentlich A, Ariel N, Bromberg A, Marcus D, et al. Acetylcholinesterase peripheral anionic site degeneracy conferred by amino acid arrays sharing a common core. *J Biol Chem.* 1994;269:6296–305.
18. Bourne Y, Taylor P, Radić Z, Marchot P. Structural insights into ligand interactions at the acetylcholinesterase peripheral anionic site. *EMBO J.* 2003;22:1–12.
19. Dorransoro I, Castro A, Martínez A. Peripheral and dual binding site inhibitors of acetylcholinesterase as neurodegenerative disease modifying agents. *Expert Opin Ther Pat.* 2003;13:1725–32.
20. Cousin X, Strähle U, Chatonnet A. Are there non-catalytic functions of acetylcholinesterases? Lessons from mutant animal models. *Bioessays.* 2005;27:189–200.
21. Inestrosa NC, Alvarez A, Perez CA, Moreno RD, Vicente M, Linker C, et al. Acetylcholinesterase accelerates assembly of amyloid- β -peptides into Alzheimer's fibrils: possible role of the peripheral site of the enzyme. *Neuron.* 1996;16:881–91.
22. Galdeano C, Viayna E, Arroyo P, Bidon-Chanal A, Ramon Blas J, Muñoz-Torrero D, et al. Structural determinants of the multifunctional profile of dual binding site acetylcholinesterase inhibitors as anti-Alzheimer agents. *Curr Pharm Des.* 2010;16:2818–36.
23. Impact Schrödinger, LLC, New York, NY, 2016; Prime, Schrödinger, LLC, New York, NY, 2016; BioLuminate, Schrödinger, LLC, New York, NY, 2016. <https://www.schrodinger.com/>. Accessed: 2019.
24. Banerjee K, Roy S, Biradha K. Design, synthesis, and photoluminescence properties of one-, two-, and three-dimensional coordination polymers: anion-assisted argentophilic interactions as building blocks. *Cryst Growth Des.* 2014;22:5164–70.
25. Vatsadze S, Manaenkova M, Sviridenkova N, Zyk N, Krut'ko D, Churakov A, et al. Synthesis and spectroscopic and structural studies of cross-conjugated dienones derived from cyclic ketones and aromatic aldehydes. *Russ Chem Bull.* 2006;55:1184–94.
26. Katritzky AR, Fan WQ, Jiao XS, Li QL. Bridged cyanine dyes. Part 3. Zwitterionic *bis*-4-pyridyl and cationic *bis*-dimethylanilino derivatives. *J Heterocycl Chem.* 1988;25:1321–5.
27. Ellman GL, Courtney KD, Andres V, Featherstone RM. A new and rapid colorimetric determination of acetylcholinesterase activity. *Biochem Pharmacol.* 1961;7:88–95.
28. Friesner RA, Banks JL, Murphy RB, Halgren TA, Klicic JJ, Mainz DT, et al. Glide: a new approach for rapid, accurate docking and scoring. 1. Method and assessment of docking accuracy. *J Med Chem.* 2004;47:1739–49.
29. Bowers KJ, Chow E, Xu H, Dror RO, Eastwood MP, Gregersen BA, et al. (2006) Scalable algorithms for molecular dynamics simulations on commodity clusters. In: *ACM/IEEE SC 2006 Conference.*
30. Jorgensen WL, Maxwell DS, Tirado-Rives J. Development and testing of the OPLS all-atom force field on conformational energetics and properties of organic liquids. *J Am Chem Soc.* 1996;118:11225–36.
31. Essmann U, Perera L, Berkowitz ML, Darden T, Lee H, Pedersen LG. A smooth particle mesh Ewald method. *J Chem Phys.* 1995;103:8577–93.
32. Lyne PD, Lamb ML, Saeh JC. Accurate prediction of the relative potencies of members of a series of kinase inhibitors using molecular docking and MM-GBSA scoring. *J Med Chem.* 2006;49:4805–8.
33. Bogan AA, Thorn KS. Anatomy of hot spots in protein interfaces. *J Mol Biol.* 1998;3(280):1–9.
34. Chaturbedy P, Kumar M, Salikolimi K, Das S, Sinha SH, Chatterjee S, Suma BS, Kundu TK, Eswaramoorthy M. Shape-directed compartmentalized delivery of a nanoparticle-conjugated small-molecule activator of an epigenetic enzyme in the brain. *J Control Release.* 2015;217:151–9.
35. Chatterjee S, Cassel R, Schneider-Anthony A, Merienne K, Cosquer B, Tzeplaeff L, Sinha SH, Kumar M, Chaturbedy P, Eswaramoorthy M, Le Gras S. Reinstating plasticity and memory in a tauopathy mouse model with an acetyltransferase activator. *EMBO Mol Med.* 2018;11:1–10.

Publisher's Note Springer Nature remains neutral with regard to jurisdictional claims in published maps and institutional affiliations.